

Computational fluid dynamics simulations of Taylor bubbles rising in vertical and inclined concentric annuli

Yixin Liu ^{a,*}, Evren M. Ozbayoglu ^a, Eric R. Upchurch ^b, Silvio Baldino ^a

^a Tulsa University Drilling Research Project, The University of Tulsa, 74104, Tulsa, OK, United States

^b Chevron Technology Company, 77002, Houston, TX, United States



ARTICLE INFO

Keywords:

Taylor bubble
Slug flow
Inclined annulus
Rise velocity
Drift velocity
Numerical simulation

ABSTRACT

Motivated by a dearth of research on the dynamics of single Taylor bubbles in annular conduits, a computational study of Taylor bubbles rising in vertical and inclined annuli is performed using a three-dimensional computational fluid dynamics (CFD) simulation with the Volume-of-Fluid (VOF) method implemented in the commercial software ANSYS Fluent (Release 19.2). The effects of Eötvös number ($Eo = [10, 300]$), inverse viscosity number ($Nf = [40, 320]$), and inclination angles ($\theta = \{10^\circ, 20^\circ, 30^\circ, \dots, 80^\circ\}$) on the steady-state Taylor bubble shape and rise velocity are investigated. The latter is parameterized by Froude number (Fr) and simulations are carried out keeping constant liquid-gas density ratio and dynamic viscosity ratio at 1000 and 100, respectively. The simulation results provide good agreement with the existing numerical findings and experimental observations. For Taylor bubbles in a vertical annulus, the surface tension and liquid viscosity show significant impacts on bubble shape (length and trailing edge) and Fr for $Eo = [10, 100]$ and $Nf = [40, 160]$. A correlation for Fr in terms of Eo and Nf is proposed and compared against 66 numerical simulations and 20 air-water experimental results available in the literature, resulting in average errors of 2.13% and 5.52%, respectively. Relatively large errors of 7.38% for characteristic dimension $D^* \leq 45$ mm and 11.82% for $D^* \geq 344.9$ mm are observed ($D^* = D_o + D_i$). The correlation exhibits improved performance with an average error of 3.5% for 45 mm $\leq D^* \leq 214$ mm relative to the only existing model. The shape of bubbles and Fr values in inclined annulus, where the bubble becomes more streamlined and unfolded, are observed to be dramatically different from those in vertical annulus. Interestingly, the wrap angle (θ_{wrap}) decreases linearly with the increase of inclination angle. Predictions of the dimensionless rise velocity in inclined annulus are made and successfully compared with an existing model and experimental data from the literature.

1. Introduction

Multiphase flow is widespread in industrial operations such as chemical reactions, nuclear reactors, and the petroleum industries. As the most common flow pattern, slug flow is observed whilst transporting hydrocarbons through pipelines, in coal seam gas (CSG) applications, and in conventional oil, gas, and geothermal drilling operations when gas bubbles migrate in the wellbore (annular conduit). The calculations of pressure drop and void fraction of slug flow as well as the gas influxes' removal with upward or downward flowing liquid during drilling operations rely primarily on capturing the migration rate of gas phase in static fluids (Liu et al., 2020; Xie et al., 2022b; Lou et al., 2022b; Luo et al., 2022). Slug flow is typically characterized by a slug unit, which is consisted of a Taylor bubble that occupies most of the cross-section area

and liquid slugs where small bubbles are entrained. Thus, understanding the motion of single Taylor bubbles is the prerequisite to modeling the complex hydrodynamics of slug flow.

As the starting point for understanding slug flow, a substantial amount of research including experimental (White and Beardmore 1962; Benjamin 1968; Bendiksen 1984; Hasan and Kabir 1988; Carew et al., 1995; Shosho and Ryan 2001; Sousa et al., 2006; Gokcal et al., 2009; Jeyachandra et al., 2012; Moreiras et al., 2014; Liu et al., 2021), theoretical (Dumitrescu 1943; Davies and Taylor 1950; Brown 1965; Grace and Harrison 1967; Viana et al., 2003; Joseph 2003; Funada et al., 2005; Fabre 2016; Lizarraga-Garcia et al., 2017; Majumdar and Das 2019), and numerical (Mao and Dukler 1990; Bugg and Saad 2002; Lu and Prosperetti 2009; Araújo et al., 2012; Gutiérrez et al., 2017; Massoud et al., 2018, 2020; Lou et al., 2020; Lizarraga-Garcia et al., 2021; Abubakar and Matar 2021) work has been conducted on the dynamics of

* Corresponding author.

E-mail address: yal8832@utulsa.edu (Y. Liu).

Nomenclature

a,b,c,d,e,f,g,h	Empirical parameters used in drift velocity correlation [-]
Ca	Capillary number [-]
CLSVOP	Coupled Level Set/Volume-of-Fluid [-]
D*	Characteristic dimension [m]
D _h	Hydraulic diameter [m]
D _i	Inner diameter [m]
D _o	Outer diameter [m]
D _η	Diameter ratio ($D_{\eta} = D_o/D_i$) [-]
Eo	Eötvös number [-]
F	surface tension force [-]
Fr	Froude number [-]
Fr ₀	Froude number for inclined conduit [-]
g	Gravitational acceleration [m/s ²]
k	curvature of the interface [-]
LBM	Lattice Boltzmann method [-]
LS	Level set [-]
L _{TB}	Taylor bubble length [m]
Mo	Morton number [-]
n	Normal vector [-]
Nf	Inverse viscosity number [-]

Ri	Inner radius [m]
Ro	Outer radius [m]
t	Time [s]
U _d	dimensional drift velocity [m/s]
U _{d0}	dimensional drift velocity measured in inclined conduit [m/s]
v	velocity vector [-]
VOF	Volume-of-fluid [-]
V _p	Parameter vector [-]
α _g	gas void fraction [-]
α _l	liquid holdup [-]
δ	Liquid film thickness [m]
θ	Inclination angle (measured from vertical) [°]
θ _w	Contact angle [°]
θ _{wrap}	Wrap angle [°]
μ _l	liquid viscosity [Pa.s]
μ _{water}	water viscosity [Pa.s]
ρ _{air}	air density [kg/m ³]
ρ _g	gas density [kg/m ³]
ρ _l	liquid density [kg/m ³]
ρ _{water}	water density [kg/m ³]
σ	Surface tension N/m

Taylor bubbles in tubular conduits. Experiments, models, and simulations reported by those studies considered the effects of fluid properties, pipe diameters, inclination angles, and bubble sizes on the rise velocity of Taylor bubble. Studies on the behavior of Taylor bubbles in annular conduits, however, are limited when compared to the research done on pipe flows.

Over the last 60 years, experimental studies of Taylor bubbles rising through stagnant fluids in an annular conduit have been conducted by several investigators (Griffith 1964; Rader et al., 1975; Sadatomi et al., 1982; Kelessidis and Dukler 1990; Hasan and Kabir 1992; Caetano et al., 1992a, 1992b; Das et al., 1998; Agarwal et al., 2007; Rohilla and Das 2019). In most oil, gas, and geothermal drilling operations, wellbores are rarely oriented vertically and contain high-density and high-viscosity drilling fluids, which highlights the limitations of existing experimental investigations that are mainly focusing on low-viscosity fluids in vertical conduits. Lou et al., (2022a) proposed a unified prediction model for Taylor bubble in the annulus filled with power-law fluids by considering the bubble shape, surrounding flow field, and energy dissipation. A recent work by Liu et al., (2022) attempted to establish a theoretical model to predict the drift velocity of Taylor bubble in non-Newtonian fluids, exhibiting a yield stress, through concentric and eccentric inclined annulus. The accuracy of this model was validated by their experimental results and other published data and showed good performance with variations in fluid properties and inclinations. However, the limitation of this model exists as it is more applicable for large annuli where surface tension has little impact on the Taylor bubble. In comparison to the experimental and theoretical methods, numerical simulations are relatively inexpensive concerning time and cost. Rohilla and Das (2017) conducted numerical simulations on the transition of Taylor bubbles from tubular pipe to an annulus using the coupled level set and volume-of-fluid (CLSVOF). Simulations of two-phase slug flow in horizontal and nearly horizontal concentric/eccentric annulus, using OpenFOAM, and applying the InterFoam method, were performed by Friedemann et al., (2019, 2020). They also compared the numerical results for pressure gradient and holdup with experimental data. Mitchell and Leonardi (2020a, 2020b) developed the lattice Boltzmann method (LBM) to study Taylor bubbles in annuli providing key insights into the effects of fluid properties, inclination, liquid flow, and geometric features such as diameter ratio and

eccentricity. A robust closure relation for Taylor bubble in vertical and inclined annulus was proposed by Mitchell and Leonardi (2020a) through the high-fidelity numerical results, which addressed the knowledge gap of surrogate model for the migration of a single Taylor bubble in an annulus that considers fluid properties.

Despite a large number of studies, there are still no extensive studies on the rise of Taylor bubbles in vertical and inclined annuli, especially using computational fluid dynamics (CFD) simulations. To achieve this goal, this study applies CFD model using the volume-of-fluid (VOF) method embedded in the commercial software ANSYS Fluent (Release 19.2). The VOF method ensures mass conservation and offers greater generality as the contemporary standard for commercial and open-source CFD software. This method has been proved to be able to accurately simulate complex multiphase flow, like slug flow, in pipes, and its application to simulate Taylor bubble motion in annulus will be presented. First, a literature review of the analysis by previous investigators is given. Then, a description of the details of the CFD model covering the mathematical equations, setup, and the numerical methods will be provided. The numerical results of the steady-state Taylor bubble moving in stagnant fluids in vertical annuli are discussed. A drift velocity correlation, characterized by the dimensionless Eötvös number (Eo), inverse viscosity number (Nf), and Froude number (Fr), for Taylor bubbles in vertical annuli is proposed, followed by the effect of inclination angle (θ) on the rise velocity and final shape of Taylor bubble. Finally, conclusions and remarks will follow.

2. Literature review

A Taylor bubble in a vertical circular tube is symmetric about the axis, in the absence of countercurrent flow. The bubble consists of a bullet-shaped, semi-spherical nose and a cylindrical body with liquid film surrounding it, followed by a wake region. In comparison to the axisymmetric shape observed in vertical pipes, when Taylor bubbles are rising in an annulus they wrap partially around the inner pipe (see Fig. 1a), shifting the shape of the bubble nose from a semi-spherical cap to an ellipsoidal front (Kelessidis and Dukler 1990; Das et al., 1998), which provides a passage for the falling fluid. A contour of the axial liquid velocity (Fig. 1b) on the plane splitting from the bubble nose to the pipe center also indicates the falling down fluid (blue color) through

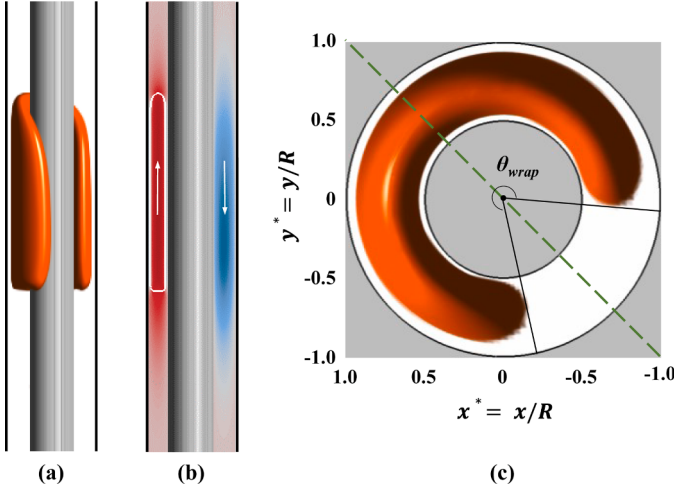


Fig. 1. Hydrodynamic features of Taylor bubble in vertical annulus. (a) steady-state shape; (b) contour of the axial liquid velocity; (c) cross-sectional bubble shape and wrap angle.

the liquid bridge and circulation (red color) in the wake region. The main objective of this study is to investigate the rise velocity of single Taylor bubbles in terms of variable properties of fluids and inclination angles in concentric annulus. Other hydrodynamic features of Taylor bubble such as bubble shape, wrap angle (Fig. 1c), and liquid film thickness will also be discussed.

As the most significant feature, the rise velocity of Taylor bubble in stagnant fluid can be expressed by the ratio of inertia to gravitational forces, parameterized by the dimensionless Froude number Fr .

$$Fr = \frac{U_d}{\sqrt{gD^*}} \quad (1)$$

where U_d is the dimensional rise velocity (aka, drift velocity); g is the gravitational acceleration while D^* is the characteristic dimension. For pipes, D^* equals the pipe diameter D and for annuli, $D^* = D_o + D_i$, where D_o and D_i represent the outer and inner diameter, respectively. $D_o + D_i$ is known as the equiperipheral diameter.

Other dimensionless numbers that govern the motion of a Taylor bubble are the Eötvös number Eo (ratio of gravitational to interfacial forces), Morton number Mo (ratio of viscous to interfacial forces), and inverse viscosity number Nf (ratio of buoyancy to viscous forces).

$$Eo = \frac{(\rho_l - \rho_g)gD_h^2}{\sigma}, Mo = \frac{(\rho_l - \rho_g)g\mu_l^4}{\rho_l^2\sigma^3}, Nf = \frac{\sqrt{(\rho_l - \rho_g)\rho_l gD_h^3}}{\mu_l} \quad (2)$$

where ρ_l and ρ_g denote the densities of liquid and gas phase, μ_l , σ , and D_h represent the liquid dynamic viscosity, surface tension, and hydraulic diameter ($D_h = D_o - D_i$), respectively.

Experiments for air and water as working fluids (Sadatomi et al., 1982; Barnea and Shemer 1986; Hasan and Kabir 1992; Das et al., 1998) with D^* greater than 38.1 mm have shown that the values of Fr vary from 0.32 to 0.36 in a vertical annulus, while for small equiperipheral diameter where $D^* < 38.1$ mm, Das et al., (1998) proposed a value of 0.246 for Fr . It should be mentioned that the authors used the outer diameter to characterize the results, whereas we use the equiperipheral diameter of an annular space throughout the paper. Table 1 summarized the literature correlations for drift velocity in vertical annulus. The characteristic dimension D^* defined by the authors has different expressions. The equiperipheral diameter D^* was used by researchers like Sadatomi et al., (1982); Caetano et al., (1992a), (1992b); Das et al., (1998); Firouzi et al., (2016); Liu et al., (2022). The average diameter of curvature ($D^* = \frac{D_o}{4} [(\pi + 1) + \frac{D_i}{D_o}(\pi - 1)]$) was proposed by Barnea and

Table 1
Drift velocity correlations for Taylor bubbles in vertical annuli.

Reference	Correlation	
Griffith (1964)	$U_d = Fr\sqrt{gD_o}$	(3)
Rader et al., (1975)	$U_d = 10C_1\sqrt{F_g}C_2C_3\sqrt{\frac{(R_o + R_i)(\rho_L - \rho_G)}{\rho_L}}$	(4)
Sadatomi et al., (1982)	$U_d = 0.345\sqrt{g(D_o + D_i)}$	(5)
Barnea and Shemer (1986)	$U_d = 0.47\sqrt{g\left(\frac{D_o}{4}\left[(\pi + 1) + \frac{D_i}{D_o}(\pi - 1)\right]\right)}$	(6)
Hasan and Kabir (1992)	$U_d = [0.345 + 0.1(D_i/D_o)]\sqrt{gD_o(\rho_L - \rho_G)/\rho_L}$	(7)
Das et al., (1998)	$U_d = \begin{cases} 0.264\sqrt{g(D_o + D_i)}, & D_o < 25.4 \text{ mm} \\ 0.323\sqrt{g(D_o + D_i)}, & D_o \geq 25.4 \text{ mm} \end{cases}$	(8)

Shemer (1986). Finally, the outer diameter was instead utilized by Griffith (1964) and Hasan and Kabir (1992). In this study, equiperipheral diameter is chosen for use as the characteristic dimension. The work of Das et al., (1998) and Liu et al., (2022) suggest this to be appropriate. Das et al.'s work showed that bubble rise velocity increases with both D_i and D_o . Similarly, after testing various characteristic dimensions in the construction of a bubble rise velocity correlation, Liu et al. determined that equiperipheral diameter yields the best performance. For a detailed evaluation of different characteristic dimensions, the interested reader is referred to Liu et al., (2022).

The impact of liquid viscosity on the rise velocity of Taylor bubble has been extensively studied in pipes (Gokcal et al., 2009; Jeyachandra et al., 2012; Moreiras et al., 2014) by performing medium and high-viscosity oil experiments. Instead of considering a single variable for fluid properties, White and Beardmore (1962) conducted experiments with various fluids associated with $Mo = [1.6 \times 10^{-11}, 1.05 \times 10^2]$, generating graphical conditions under which the viscous force and surface tension force may be neglected. In general, their results suggest that surface tension and viscosity have no impact on bubble velocity when $Eo > 70$ and $Nf > 550$. Also, rise velocity has little dependence on the inertial force if $Fr < 0.003$. Recent work of Viana et al., (2003) denotes marginally different limits where surface tension and liquid viscosity are irrelevant to bubble velocity: $Eo > 40$, $Nf > 200$. A universal correlation [Eq. (9)] for Fr in terms of Eo and Nf is developed by Viana et al. with data from 255 existing experiments and seven new experiments. Other observations, such as that the rise velocity is independent of the length of the gas bubble and how it is introduced, are also remarked, in line with the experimental studies (Polonsky et al., 1999; Sousa et al., 2006; Agarwal et al., 2007; Liu et al., 2021).

$$Fr = \frac{0.34 / \left[1 + (14.793/E_o)^{3.06} \right]^{0.58}}{\left(1 + \left[\frac{N_f}{31.08 \left((1 + 29.868/E_o)^{1.96} \right)^{0.49}} \right]^A \right)^B} \quad (9)$$

$$A = -1.45 \left(1 + (24.867/E_o)^{9.93} \right)^{0.094}$$

$$B = -1.0295/A$$

Inspired by Viana et al., Mitchell and Leonardi (2020a) proposed a closure relation of Fr for Taylor bubbles rising in vertical annulus with high-fidelity data using the lattice Boltzmann method (LBM). This model shares a similar but more simplified form of Eq. (9) and retains the power-laws in Eo . It is worth noting that Eq. (10) is slightly different from that shown in the original paper. The authors have verified that the original publication appears to be missing a set of brackets (now shown here).

$$Fr = \frac{0.383 / \left[1 + (1.4078/E_o)^{0.6442} \right]^{1.5381}}{\left(1 + \left[\frac{N_f}{(3.6321(1 - 1.5753/E_o))^{2.7688}} \right]^{-1.1635} \right)} \quad (10)$$

Experimental studies (Zukoski 1966; Bendiksen 1984; Weber et al., 1986; Hasan and Kabir 1988; Carew et al., 1995; Liu et al., 2021) and numerical work of Lizarraga-Garcia et al., (2017) have been done on the drift velocity of Taylor bubbles in inclined pipes. Generally, the drift velocity increases with the inclination angle increasing and then decreases, reaching a maximum value between 30° and 60° from vertical.

Bendiksen (1984) correlated the drift velocity for inclined flow by combining the vertical (U_d^v) and horizontal (U_d^h) drift velocities. It was then adopted by other investigators (Petalas and Aziz 2000; Jeyachandra et al., 2012) as the mainstream correlation.

$$U_{d\theta} = U_d^v \cos\theta + U_d^h \sin\theta \quad (11)$$

The expression of drift velocity for upward inclined flow reported by Gockal et al., (2009) stemmed from Bendiksen's correlation.

$$U_{d\theta} = U_d^v (\cos\theta)^{0.7} + U_d^h (\sin\theta)^{1.5} \quad (12)$$

Published research on inclined annular pipe flow experiments is limited, only three of the studies (i.e., Rader et al., 1975; Hasan and Kabir 1992; Liu et al., 2022) provide insights into the influence of inclination on bubble behavior in the annular conduits. Rader et al. measured the annular bubble rise velocity in stagnant water columns at various deviations from vertical and the maximum velocity occurred at 45°. The authors pointed out that the mutual restriction of the variation in drag force and gravitational force with θ causes the change in velocity with θ to firstly increase and subsequently decrease. Hasan and Kabir (1988, 1992) proposed a drift velocity correlation [Eq. (13)] for small pipe and annulus diameter, deviated between 0° and 32° from vertical. This expression predicts zero rise velocity for horizontal annulus and it is indicated by the authors that Eq. (13) appears to over-predict $U_{d\theta}$ when the conduit is highly deviated from vertical. In our previous study (Liu et al., 2022), experiments have been conducted capturing the $U_{d\theta}$ in stagnant Bingham plastic fluids in an inclined (4°, 15°, 30°, 45°) and fully eccentric 0.1524×0.1016 m (6 × 4-in) annulus. $U_{d\theta}$ is found to be generally maximized at θ of ~30° and a similar correlation with Gockal et al. provides the most accurate performance for predicting the effect of θ .

$$U_{d\theta} = U_d^v \sqrt{\cos\theta} (1 + \sin\theta)^{1.2} \quad (13)$$

Numerical simulation has been extensively applied for the analysis of the bubbles rising in pipes. Different methods include VOF (Kawaji et al., 1997; Cook and Behnia 2001; Taha and Cui 2006; Araújo et al., 2012; Massoud et al., 2018, 2020), Level Set (Liné et al., 2013; Lizarraga-Garcia et al., 2017, 2021; Gutiérrez., 2017), Coupled Level Set/Volume-of-Fluid (CLSOVOF) method (Ohta et al., 2008; Keshavarzi et al., 2014), Front Tracking method (Hua and Lou 2007; Lu and Prosperetti 2009; Kang et al., 2010; Quan 2011) are used to track the phase interface. More recently, Abubakar and Matar (2021) studied the steady-state Taylor bubbles in stagnant and flowing liquids in vertical pipes using a Galerkin finite-element method implemented in FreeFem++. The authors concluded that surface tension and viscosity have a strong influence on the bubble nose and bottom curvature below the limits $Eo = [20, 30]$ and $Nf = [60, 80]$.

In comparison with the ample computational studies focused on Taylor bubbles in pipes, only two research groups Rohilla and Das (2017) and Mitchell and Leonardi (2020a, 2020b), mentioned in the last section, have sought to explore the motion of Taylor bubbles in annulus. Additionally, literature about the experimental and theoretical studies on this topic is deficient, which provides the key motivation for this work.

3. CFD model development

In this study, the Volume-of-Fluid (VOF) method implemented in ANSYS Fluent (Release 19.2) is utilized to track the interface between two phases, and the following equations are solved for continuity,

momentum, and volume fraction calculation. Details about those governing equations can be found in the software literature.

3.1. Mathematical model

In the absence of mass transfer between phases, the continuity and momentum equations are:

$$\frac{\partial \rho}{\partial t} + \nabla \cdot (\rho v) = 0 \quad (14)$$

$$\frac{\partial(\rho v)}{\partial t} + \nabla \cdot (\rho vv) = -\nabla p + \nabla \cdot [\mu(\nabla v + \nabla^T v)] + \rho g + F \quad (15)$$

where t is the time; v is the velocity vector; ρ and p are the density and pressure, respectively; $[\mu(\nabla v + \nabla^T v)]$ is the viscous stress tensor; g is the gravity vector; and $F = \sigma k \frac{\rho \nabla \alpha_g}{0.5(\rho_g + \rho_l)}$ is the surface tension term based on the continuum surface force (CSF) model (Brackbill et al., 1992).

The curvature of the interface, k , is expressed as the divergence of the unit vector normal.

$$k = \nabla \cdot n \quad (16)$$

where n is the unit vector normal to the interface, computed based on the gas phase volume fraction.

$$n = \frac{\nabla \alpha_g}{\| \nabla \alpha_g \|} \quad (17)$$

We assume that the two phases are incompressible and immiscible and the void fraction is only solved for the secondary phase, which is used to calculate the mixture density and viscosity.

$$\rho = \rho_l \alpha_l + \rho_g \alpha_g \quad (18)$$

$$\mu = \mu_l \alpha_l + \mu_g \alpha_g \quad (19)$$

The Volume of Fluid (VOF) method was adopted (Hirt and Nichols, 1981) as the interface tracking technique by solving the conservation equation for the volume fraction function.

$$\frac{\partial \alpha_g}{\partial t} + v \cdot \nabla \alpha_g = 0 \quad (20)$$

3.2. Test matrix and computational domain setup

In this study, single Taylor bubbles rising in vertical and inclined annulus with stagnant fluids were simulated, covering a wide range of fluid properties characterized by the dimensionless Eötvös number $Eo = [10, 300]$, inverse viscosity number $Nf = [40, 320]$, and resultant Froude number Fr . In some cases, for Eo and Nf values higher than used in this study, numerical imbalances originated from inside the bubble and driven by the bubble pressure resulted in spurious velocities at the discretized level – manifesting itself as waviness on the Taylor bubble boundary. To prevent the occurrence of this numerical instability within our chosen parameter space, a smaller time-step size and finer mesh were applied for high Eo and high Nf cases (i.e., $Eo \geq 220$, $Nf \geq 240$), and the corresponding Capillary number $Ca = \mu U_d / \sigma = [0.64, 1.15]$ can be obtained. A total of 66 cases (see Fig. 2) are simulated for vertical annulus.

For inclined cases, simulations were run for $Eo = \{20, 60, 100, 140\}$ and $Nf = \{40, 80, 160, 320\}$ for $\theta = [0^\circ, 80^\circ]$. Consequently, a large numerical database was generated to investigate the effect of fluid properties and inclination angle on the motion of Taylor bubble in an annulus.

The computational domain is a three-dimensional concentric annulus with a diameter ratio of 2 ($D_\eta = D_o/D_i = 2$), and a length of $11D_o$ to ensure no end-effects on the solutions. Initially, the bubble's bottom is placed $1.5D_o$ from the bottom of the annulus, has an axisymmetric shape

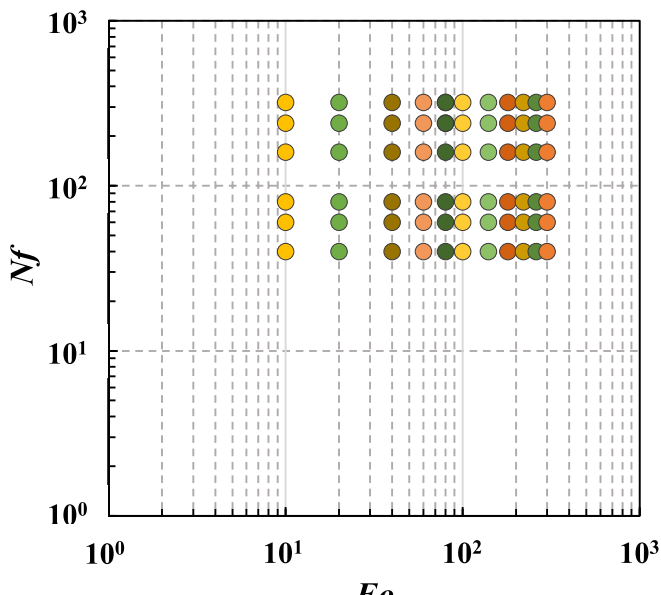


Fig. 2. Test matrix map for vertical cases.

of hemisphere nose and cylindrical body, and a length of $L_{TB} = 2D_o$. To ensure the development of liquid film, there are 10 or 8 cells between the cylindrical bubble surface and pipe walls, depending on the mesh type. These initial conditions apply for all simulations and are verified to not impact the final rise velocity, bubble nose shape, and wrap angle obtained by the simulation's end (Das et al., 1998; Polonsky et al., 1999; Gutiérrez et al., 2017; Mitchell and Leonardi, 2020b). The initial Taylor bubble shape and the computational domain are shown in Fig. 3. To

examine the effect of Eo and Nf on the motion of a Taylor bubble, the liquid-gas density ratio and the dynamic viscosity ratio were fixed at 1000 and 100 (Mitchell and Leonardi, 2020a), respectively. The boundary conditions are (1) no-flow wall at the bottom of the annulus, (2) flow allowed at the top of the annulus, (3) no-slip at the pipe walls, and (4) all the velocity components are set as zero ($u = v = w = 0$). The gravity vector is adjusted to reflect the chosen annulus inclination angle. The non-uniform mesh was applied with mesh refinement near the wall. The structured mesh size is analyzed and refined until the terminal velocity converges (Xie et al., 2022a).

3.3. Numerical solution methods

The pressure-based segregated algorithm (PRESTO!) is applied to solve the transport equations for the pressure equation. The Pressure Implicit with Splitting of Operators (PISO) algorithm with the skewness correction is adopted as the pressure-velocity coupling scheme to significantly reduce the convergence difficulties associated with highly distorted meshes. The Least Squares Cell Based method is used for the gradient discretization. The Geo-Reconstruct scheme is employed for interface tracking, while first-order implicit method is applied to set different time-dependent solution formulation. To avoid the numerical instability issue at a high density ratio, the second-order upwind scheme was used for spatial discretization to obtain more accurate results, especially for cases where the flow direction is not aligned with the grid. The absolute convergence criterion of 10^{-4} was set for continuity and velocities, with a maximum number of iterations of 1000. A variable time step was utilized for the governing equations for a global Courant number of 0.25.

4. Results and discussions

4.1. Mesh independence study

To determine the dependence of the results on the mesh density (Zhu et al., 2019), four different mesh types (see Fig. 4) named coarse, medium, fine, and finer were used to simulate the experimental work of Sadatomi et al., (1982) with an air-water system in vertical annulus. The outer and inner diameters are 0.03 m and 0.015 m, respectively. The corresponding dimensionless numbers are: $Eo = 30.58$, $Nf = 5739$, $Fr = 0.3176$. For all air-water experiments considered in this study, the fluid properties are assumed to be: $\rho_{water} = 998 \text{ kg/m}^3$, $\rho_{air} = 1.225 \text{ kg/m}^3$, $\mu_{water} = 0.001 \text{ Pa.s}$, $\mu_{air} = 0.00001 \text{ Pa.s}$ and $\sigma = 0.072 \text{ N/m}$. Fig. 5 shows the evolution of Fr over time for different mesh types. The simulation results and errors are presented in Table 2. The results indicate that Fr tends to be stabilized more rapidly when a finer mesh is applied. The average errors for the fine and finer mesh types are 1.06% and 0.08%, respectively. In the trade-off between the accuracy and simulation time, either finer or fine mesh type was employed depending on the annulus geometry.

4.2. CFD model validation

The numerical code was validated by simulating three cases from the experimental work of Das et al., (1998) and Rader et al., (1975) on a Taylor bubble rising through concentric annulus filled with water. Different annulus dimensions were thus considered to assess the robustness of the CFD model. Table 3 summarizes the annulus geometries, dimensionless parameters, and the dimensional rise velocities.

The experimental Froude number Fr_{exp} and the simulation results Fr_{sim} , along with the errors are shown in Table 4. The predicted values Fr_{Das} , Fr_{MEL} from the models of Das et al., (1998) and Mitchell and Leonardi (2020a), respectively, and the numerical results Fr_{LBM} using the lattice Boltzmann method (LBM) published in the work of Mitchell and Leonardi (2020b) are also included. It is evident that the CFD model can accurately capture the experimental results for Cases 2 and 3 and

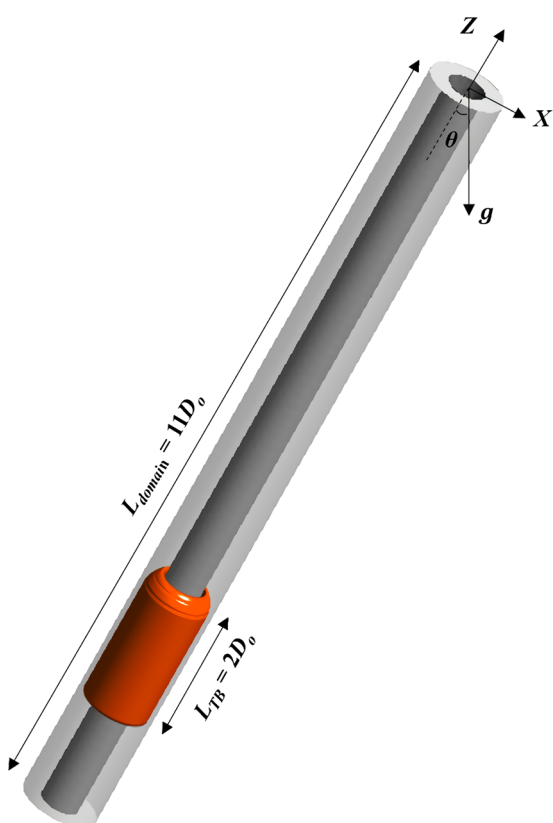


Fig. 3. Initial Taylor bubble in the computational domain.

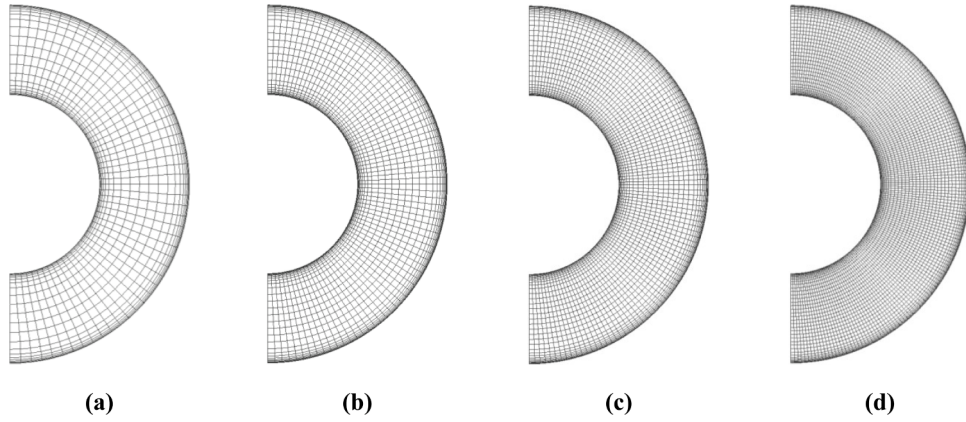


Fig. 4. Cross-section concentric annulus mesh. (a) Coarse; (b) Medium; (c) Fine; (d) Finer.

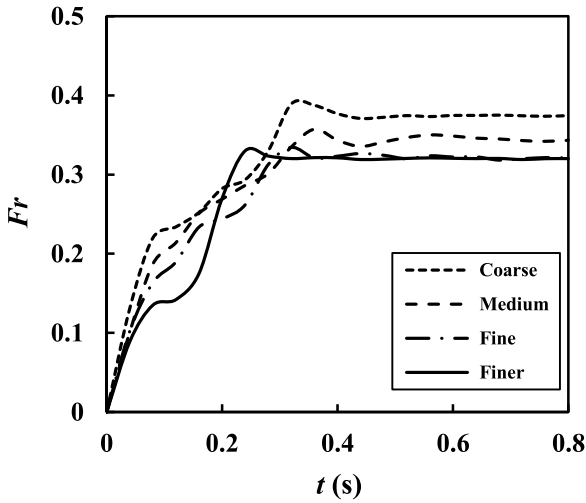


Fig. 5. Evolution of Fr over time for different mesh types.

Table 2

Simulation results and errors time for different mesh types.

Mesh type	No. of cells - radial	No. of cells - axial	No. of cells - circumferential	Fr	Error (%)
Coarse	37	367	79	0.3746	17.95
Medium	45	550	120	0.3433	8.1
Fine	53	733	157	0.3210	1.06
Finer	70	1100	236	0.3201	0.08

Table 3

Annular configurations, relevant dimensionless numbers, and rise velocities for CFD model validation purposes.

Case	Reference	D_o (m)	D_i (m)	D_h	D_o/D_i	Eo	Mo	Nf	U_d (m/s)
1	Rader et al., (1975)	0.01905	0.0127	0.0064	1.5	5.4762	2.6303E-11	1580.735	0.1311
2	Das et al., (1998)	0.0254	0.0127	0.0127	2.0	21.9049	2.6303E-11	4470.992	0.1699
3	Das et al., (1998)	0.0381	0.0127	0.0254	3.0	87.6196	2.6303E-11	12645.876	0.238

Table 4

Numerical results in comparison with experimental Fr and predictions from Das et al., 1998; Mitchell and Leonardi (2020a, 2020b).

Case	Fr_{exp}	Fr_{sim}	Error (%)	Fr_{Das}	Error (%)	$Fr_{M&L}$	Error (%)	Fr_{LBM}	Error (%)
1	0.2348	0.2555	8.78	0.246	4.75	0.2232	4.96	0.262	11.5
2	0.2779	0.2836	2.05	0.2603	6.33	0.2997	7.85	0.2770	0.6
3	0.3371	0.3383	0.36	0.3252	3.54	0.3449	2.29	-	-

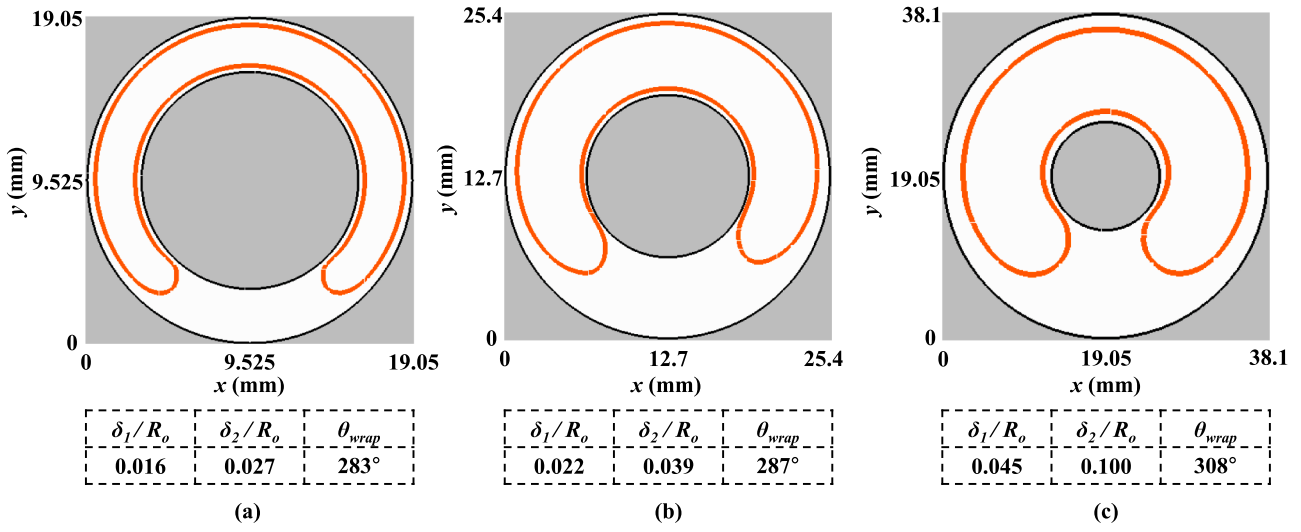


Fig. 6. Cross-sectional Taylor bubble shape, inner (δ_1 / R_o) and outer (δ_2 / R_o) liquid film thickness, and wrap angle for (a) Case 1; (b) Case 2; (c) Case 3.

Therefore, they will not be used to calculate the numerical wrap angles in this paper.

4.3. Taylor bubble in vertical annulus

In the present study, the drift velocity of Taylor bubble is measured by tracking the bubble nose and the velocity is recorded until the final steady-state is achieved. Fig. 7 provides a selected case of the time evolution of the Taylor bubble in a vertical annulus for $Eo = 60$ and $Nf = 80$. In this case, the initial axisymmetric Taylor bubble rises along one side of the annulus occupying a portion of the inner pipe and this favored side is chosen randomly (Das et al., 1998). The formation of the liquid bridge that allows fluid to flow down can also be seen.

The influence of Nf on the fully-developed Taylor bubble shape and dimensionless drift velocity at fixed $Eo = 60$ is illustrated in Fig. 8 (a). For a constant Eo , when the viscous force on the Taylor bubble diminishes due to the increase of the Nf , the Fr increases. Attributed to a drop in viscous normal stress, the length of Taylor bubble decreases marginally with Nf . It can also be noted from Fig. 8a that the bubble tail adjacent to the liquid bridge stretched with the increase of Nf , eventually breaking off and entraining small bubbles at $Nf = 320$ due to the turbulent motion of the low-viscosity fluid in the bubble's wake. Those observations correspond to the Taylor bubble experiments/simulations with low-viscosity systems (White and Beardmore, 1962; Nogueira et al., 2006; Llewellyn et al., 2012; Liu et al., 2021, 2022; Araújo et al., 2012; Lizarraga-Garcia et al., 2021; Abubakar and Matar, 2021), where small bubbles entrained in the Taylor bubble's wake (just like Fig. 8a) – and that increases in viscosity damped or eliminated the effect.

Fig. 8 (b) shows the effect of surface tension force characterized by Eo for a constant value of $Nf = 60$ on the Taylor bubble. For low Eo (e.g., $Eo = 10$), the influence of surface tension force is significant, reflected by the convex shape of the bubble's trailing edge and its compressed length. Increasing Eo makes the bubble more deformable due to decreasing surface tension. This results in a longer bubble and a transition of the Taylor bubble's trailing edge from a convex ($Eo = 10$) to a concave shape. The dimensionless rise velocity and bubble length then become weakly relevant to Eo at larger values of Eo . Unlike what was observed for the case of Taylor bubble in pipes, where the bubble swells in the region near the bottom within the range of $Eo < 20$ and becomes more noticeable as Nf increases (Araújo et al., 2012; Abubakar and Matar 2021), when a Taylor bubble rises in an annulus, the formation of the liquid bridge creates the primary pathway for liquid drainage, which avoids the emergence of the bulge.

Fig. 9 further exhibits the cross-sectional bubble profiles. The cross

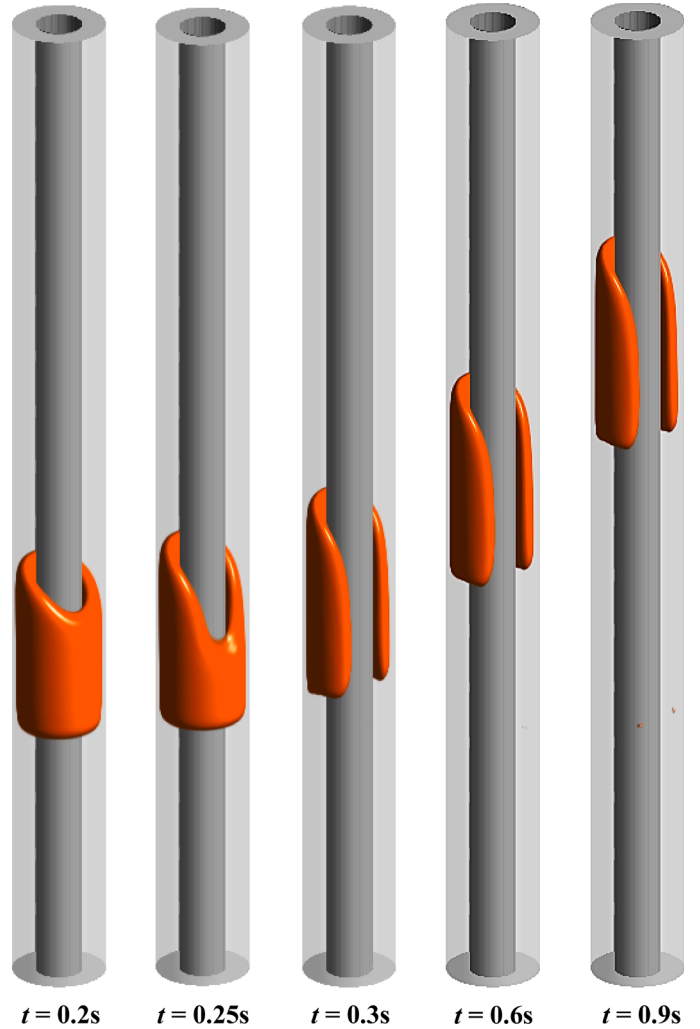


Fig. 7. Evolution of Taylor bubble in vertical annulus for $Eo = 60$ and $Nf = 80$.

section is taken from the XY plane where the wrap angle remains essentially constant along a section of the bubble. As can be seen from Fig. 9 (a) – (d), for a constant value of Eo the wrap angle slightly increases with Nf as represented by an increase in the fraction occupied by

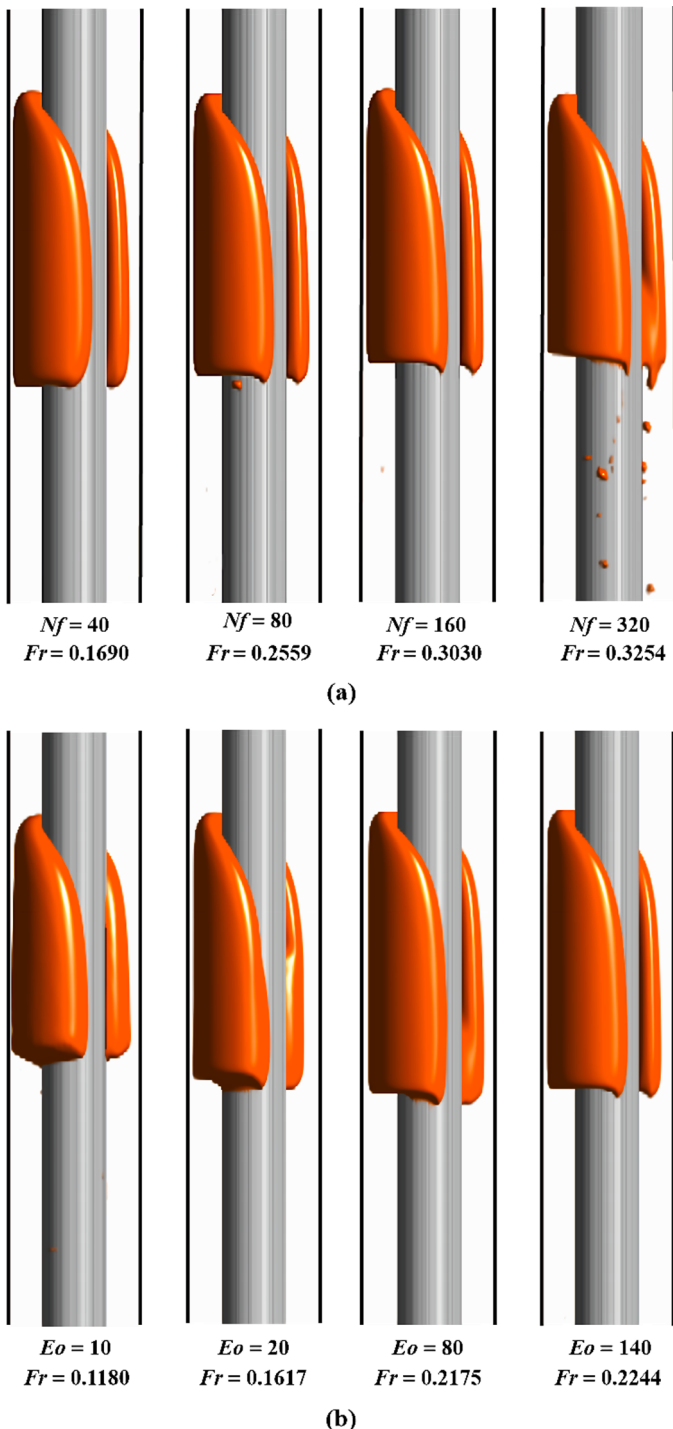


Fig. 8. Fully-developed bubble shape and dimensionless rise velocity in vertical annulus (a) effect of N_f for $E_o = 60$; (b) effect of E_o for $N_f = 60$.

the Taylor bubble around the inner pipe. The wrap angles for varying N_f are: $\theta_{wrap} = \{275^\circ, 281^\circ, 290^\circ, 293^\circ\}$. The reduction in the magnitude of the viscous force applied to the bubble as the fluid viscosity decreases causes the θ_{wrap} to increase with N_f . The variation in θ_{wrap} is more obvious when the surface tension effect is significant for small values of E_o shown in Fig. 9 (e) and (f). For each E_o , $\theta_{wrap} = \{252^\circ, 277^\circ, 283^\circ, 285^\circ\}$. This, as mentioned previously when addressing the effect of E_o on the bubble length, is because of the decrease in resistance to deformation.

The dimensionless drift velocity correlation for Taylor bubbles in vertical annulus proposed by Mitchell and Leonardi (2020b) was built

based on the tubular velocity model of Viana et al., (2003), which was developed with numerous fluid properties. Mitchell and Leonardi's correlation shows high accuracy with an average error of 2.95% within the range of parameters studied by them. However, in an air-water system with a characteristic dimension larger than 175 mm, relatively large errors on the order of 15% occur between the model and experimental results. Considering the small amount of work related to annular flow, the proposed correlation is modified from the model of Mitchell and Leonardi (2020a). The main modification is an addition of an exponential term related to E_o , on a similar basis to the original power-law type of Fr .

$$Fr = \frac{a / [1 + b / E_o + c e^{(d E_o)}]}{\left(1 + \left[\frac{N_f}{(e(1+f/E_o))^g}\right]^h\right)} \quad (24)$$

These parameters are obtained by solving the $\min(\sum \|Fr(E_o, N_f) - Fr_{sim}\|^2)$, where Fr_{sim} are the simulation results. The vector V_p containing the parameters is optimized as follows,

$$\begin{aligned} V_B &= [a, b, c, d, e, f, g, h] \\ &= [0.3495, 3.335, 7.459, -2.239, 5.216, 3.201, 2.164, -1.584] \end{aligned}$$

In Fig. 10, the numerical results for Fr are presented as a function of E_o and N_f , while the solid lines are the predictions from the proposed correlation. As shown, the proposed correlation demonstrates a high accuracy predictive performance with an average error of 2.13%. In general, increasing E_o or N_f by reducing the surface tension or viscosity results in the decrease of drag force, as indicated by the increases in Fr . It is also evident that Fr increases markedly at low E_o values, and becomes independent of E_o when E_o exceeds 100, and this critical value of E_o increases with decreasing N_f . Similarly, Fr increases as an increment in N_f and becomes stable at large N_f for a fixed E_o . This structure of the numerical data is consistent with the work of Mitchell and Leonardi (2020b) for annular Taylor bubble flow and Abubakar and Matar (2021) for tubular Taylor bubble flow. It is worth noting that in Abubakar and Matar's work, the authors point out that when $E_o < 20$, varying N_f has a marginal influence on the bubble velocity, while the change of Fr with E_o is significant in this interval. The authors' possible explanation involves the curvature of the bubble nose in the round pipe, which is outside the scope of this research. As inferred from Fig. 10, however, the change of Fr with N_f is also obvious when the E_o is low, as the Taylor bubble rises in annulus where its nose grows into an elliptic rather than a semi-spherical cap.

Due to a lack of experimental data covering the range of dimensionless parameters considered in this study, a reliable and validated air-water experimental dataset from seven references was used for model validation purposes. Those data cover the range of D^* from 19.8 mm to 445.5 mm, D_h from 6.4 mm to 141.7 mm, and D_η from 1.2 to 8.6. The relevant dimensionless numbers, experimental Fr , and the errors associated with the predicted Fr from Eq. (24) are summarized in Table 5.

Fig. 11 displays the E_o / N_f spaces used for constructing and applying the proposed correlation [Eq. (24)]. The optimized correlation is applied to a range of E_o and N_f (and their corresponding Fr numbers) in Table 5 that stretches 1 and 2.5 orders of magnitude, respectively, beyond that used to construct the correlation. In this way, we are stress-testing the correlation's range of applicability. Since all tests listed in Table 5 are for air-water experiments, the logarithmically linear, $\frac{3}{4}$ sloping E_o / N_f trend is to be expected - and simply reflects the singular dependency of E_o and N_f on the value of D_h .

The proposed model provides an accurate predictive performance in the cases of $45 \text{ mm} \leq D^* \leq 214 \text{ mm}$ with an average error of 3.5% (Fig. 12b region ②), while for cases of D^* outside this range, relatively large errors of 7.38% ($D^* \leq 45 \text{ mm}$, Fig. 12b region ①) and 11.82% ($D^* \geq 344.9 \text{ mm}$, Fig. 12b region ③) can be observed. In Fig. 12 (a), we compared the proposed correlation and existing models with the experimental data in Table 5. The models proposed by Das et al., (1998)

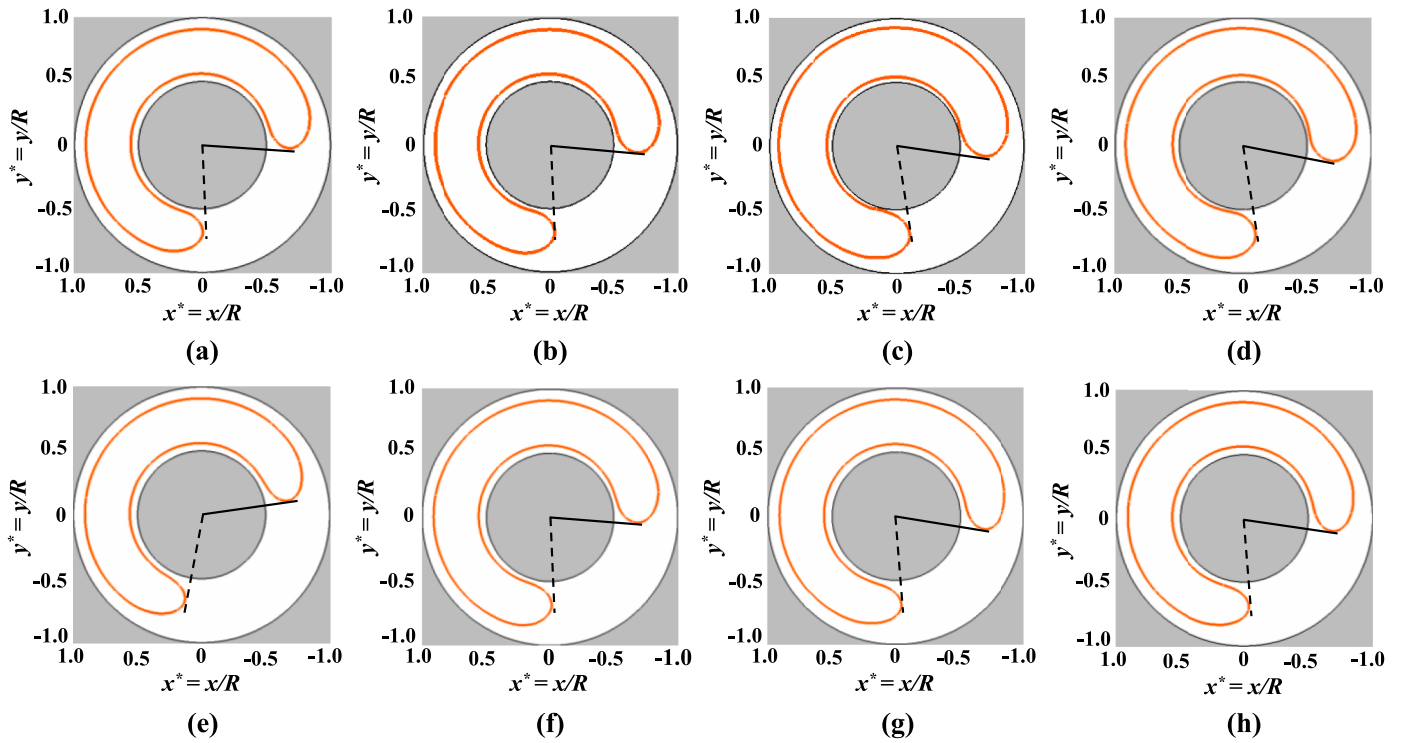


Fig. 9. Cross-sectional bubble profiles for $Eo = 60$, (a) $Nf = 40$; (b) $Nf = 80$; (c) $Nf = 160$; (d) $Nf = 320$, and for $Nf = 60$, (e) $Eo = 10$; (f) $Eo = 20$; (g) $Eo = 80$; (h) $Eo = 140$.

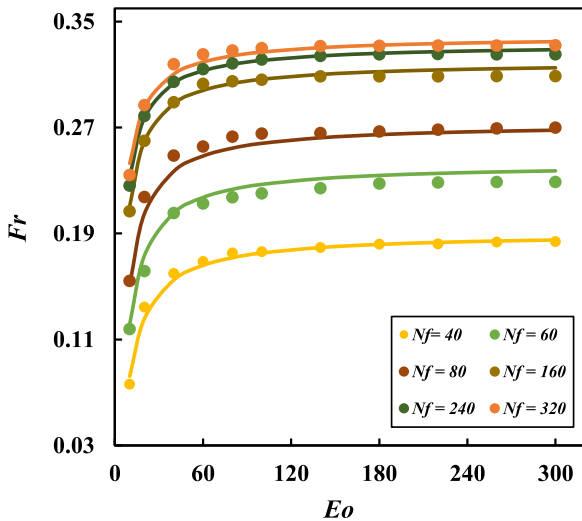


Fig. 10. Fr predictions – numerical simulation (●) versus proposed correlation [Eq. (24)] (—).

and Mitchell and Leonardi (2020a) are selected. As can be seen from Fig. 12a, the model of Das et al., (1998) was in close agreement with the experimental values, predicting Fr within the error range of 10%. This is primarily because the rise velocity model proposed by Das et al., (1998) is based on an analytical model where a modified inviscid flow analysis has been conducted. An overall agreement between the measured Fr and those from Mitchell and Leonardi's model can be obtained with an average error of 6.84%, except for those values from D^* between approximately 175 mm and 214 mm with errors of around 15%. The improvement of the accuracy can be seen by the proposed correlation with errors of about 7.36% for D^* in this range. It should be emphasized that the comparison is intended just to compare the available experimental data to the existing models, not a comprehensive model

performance assessment.

4.4. Taylor bubble in inclined annulus

The effect of inclination angle on Taylor bubbles in annulus for the following parameters: $Eo = \{20, 60, 100, 140\}$, $Nf = \{40, 80, 160, 320\}$, $\theta = \{10^\circ, 20^\circ, 30^\circ, \dots, 80^\circ\}$ is studied. The inclinations considered cover most oil, gas, and geothermal industrial scenarios. Two selected simulation cases with $Eo = 20$, $Nf = 40$ and $Eo = 60$, $Nf = 80$ are presented in Fig. 13 (a) and 13 (b), respectively, at various inclination angles. As the steady-state bubble shapes are shown in Fig. 13, the bubble nose becomes more streamlined and the tail gets elongated due to a reduction in the longitudinal buoyancy force acting on the bubble, resulting in a reduction in the drag force (interfacial force and viscous force) and growth in the length of the Taylor bubble. In addition, the bubble body is observed to unfold and be forced towards the uppermost wall as the transverse buoyancy forces increase with the inclination angle, leading to drag force and wrap angle decreases. This also contributes to bubble elongation as inclination increases.

Fig. 14 depicts the cross-sectional Taylor bubble profile dependence on inclination angle. It is more intuitive from Fig. 14 that the wrap angle of the Taylor bubble decreases linearly with an increasing annulus inclination. To the best of the authors' knowledge, this is the very first-time such behavior has been observed. The impact of inclination angle on the liquid film thickness can be reflected from the magnified regions, for which the transverse buoyancy force presses the bubble against the upper pipe wall causing the outer liquid film thickness to reduce. In contrast, changes in θ lead to a negligible influence on the liquid film thickness on the inner pipe.

When Taylor bubbles rise in the inclined annulus, their shapes change significantly as compared with the vertical case. The cross-sectional area occupied by the bubble is substantially reduced, and so is the drag force. Thus, initially, bubble velocity increases with inclination. Longitudinal buoyancy forces, however, decrease with inclination, resulting in a decreasing bubble velocity at higher inclinations

Table 5Comparison between the predicted Fr from Eq. (19) and air-water experimental data ($Mo = 2.6303E-11$).

Reference	D_o (m)	D_i (m)	D^* (m)	Eo	Nf	U_d (m/s)	Fr_{exp}	Fr_{pred}	Error (%)
Das et al.	0.0508	0.0254	0.0762	87.6196	12645.876	0.2890	0.3343	0.3368	0.76
	0.0381	0.0127	0.0508	87.6196	12645.876	0.2380	0.3371	0.3368	0.10
	0.0254	0.0127	0.0381	21.9049	4470.992	0.1699	0.2779	0.3036	9.25
Hasan and Kabir	0.1270	0.0570	0.1840	665.4719	57855.600	0.4349	0.3237	0.3478	7.44
	0.1270	0.0870	0.2140	217.2970	24991.270	0.4615	0.3185	0.3443	8.09
	0.1270	0.0480	0.1750	847.5939	69364.775	0.4270	0.3259	0.3481	6.83
Kelessidis and Dukler	0.0762	0.0508	0.1270	87.6196	12645.876	0.3700	0.3315	0.3368	1.61
Caetano et al.	0.0762	0.0422	0.1184	156.9970	19584.691	0.3540	0.3285	0.3423	4.21
Griffith	0.0508	0.0178	0.0686	147.8977	18727.045	0.2720	0.3316	0.3419	3.11
	0.0508	0.0123	0.0631	201.3053	23598.774	0.2720	0.3457	0.3439	0.54
	0.0508	0.0059	0.0567	273.7955	29721.304	0.2470	0.3312	0.3453	4.27
Sadatomi et al.	0.0300	0.0150	0.0450	30.5574	5738.987	0.2110	0.3176	0.3154	0.70
Rader et al.	0.0508	0.0320	0.0828	48.0009	8052.581	0.2926	0.3247	0.3270	0.72
	0.1412	0.0660	0.2072	768.0143	64420.650	0.4633	0.3250	0.3480	7.09
	0.0147	0.0051	0.0198	12.5685	2947.548	0.1188	0.2697	0.2764	2.48
0.0147	0.0081	0.0228	5.8623	1663.590	0.1158	0.2447	0.2214	9.53	
0.0191	0.0127	0.0318	5.4762	1587.34	0.1311	0.2348	0.2155	8.26	
0.2433	0.1016	0.3449	2726.9260	166629.970	0.7376	0.4010	0.3491	12.95	
0.2433	0.1417	0.3850	1401.9130	101167.010	0.7376	0.3795	0.3487	8.13	
0.2433	0.2022	0.4455	229.4126	26029.215	0.8412	0.4024	0.3445	14.37	

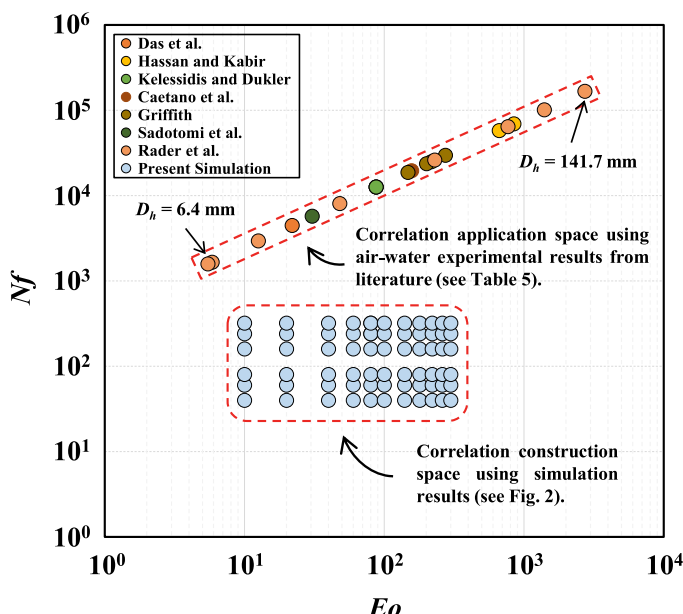


Fig. 11. Eo / Nf combinations used for constructing and applying the proposed correlation [Eq. (19)]. Corresponding Fr numbers are found in Fig. 10 and Table 5, respectively.

(usually $> 30\text{--}60^\circ$, depending on rheology). This non-monotonic variation in the velocity of Taylor bubbles with varying inclination angles in pipes has been established by extensive prior studies (Zukoski 1966; Rader et al., 1975; Bendiksen 1984; Weber et al., 1986; Hasan and Kabir 1988; Alves et al., 1993; Gokcal et al., 2009; Jeyachandra et al., 2012; Lizarraga-Garcia 2016) and various correlations for dimensionless drift velocity in inclined pipes have been proposed. On this basis, Mitchell and Leonardi (2020a) extended Bendiksen's correlation to an annular system by applying their vertical Fr model [Eqn. (10)] and the following correlation form to obtain Fr for any inclination.

$$Fr_\theta = Fr \cos\theta + (Fr)^\alpha \sin\theta \quad (25)$$

where Fr_θ is the dimensionless velocity in an inclined annulus. Correlation performed accurately at $\alpha = 1.25$ with an average error of 6.0% for the range of parameters covered in Mitchell and Leonardi (2020a)'s study.

A model similar to Bendiksen (1984) and Mitchell and Leonardi (2020a) correlations is proposed for the dimensionless drift velocity of Taylor bubble in inclined annulus. Fr is calculated from Eqn. (24), the horizontal dimensionless velocity is obtained by Fr using the same index value of 1.25 as Mitchell and Leonardi (2020a). Two coefficients associated with θ are introduced and found to be 0.89 and 0.78 after optimization.

$$Fr_\theta = Fr(\cos\theta)^{0.89} + (Fr)^{1.25} (\sin\theta)^{0.78} \quad (26)$$

The numerical results for Fr_θ and the predictions from Eq. (26) are plotted in Fig. 15. The dimensionless drift velocity increases as the inclination angle increases, peaking at approximately $30^\circ - 40^\circ$ from vertical and then decreasing to a minimum. It is apparent that Eq. (26) provides accurate estimations in comparison with the numerical outcomes. Cases for $\theta = [60^\circ, 70^\circ, 80^\circ]$ deliver relatively large errors of 7.02% and the accuracy improves with decreasing inclination angle for $\theta = [0^\circ, 10^\circ, 20^\circ]$ and $\theta = [30^\circ, 40^\circ, 50^\circ]$ with average errors of 4.04% and 5.56%, respectively.

A comparison of the proposed model [Eq. (26)] with Mitchell and Leonardi's [Eq. (25)] is illustrated in Fig. 16. The dash lines and the dash-dot lines represent the error bands of $\pm 5\%$ and $\pm 10\%$, respectively. Good agreement between the proposed model and simulation results is obtained, with the majority of the predictions lying near the 100% agreement line. In the region of high Froude number $Fr_\theta > 0.35$, the proposed model tends to slightly underestimate the numerical data obtained with large Nf at $30^\circ < \theta < 50^\circ$.

To further assess the extensibility of the proposed model, the experimental data from Rader et al., (1975) is applied. The inner and outer diameters are 0.01905 m and 0.0127 m, respectively. The air and water are the working fluids. The corresponding dimensionless numbers are: $Eo = 5.4764$, $Mo = 2.633e-11$, and $Nf = 1580.76$. Fig. 17 demonstrates the experimental and calculated Fr_θ as a function of θ . It is clear that the proposed model consistently under-predicts Rader et al.'s experimental results with an average error of 8.75%. This outcome is expected. Correlations like Eq. (26) are tuned using its three exponents to fit data sets with a restricted range of Eo and Nf values. In this case, our simulations assume a significantly higher viscosity ($Nf = 40 - 320$) than that of Rader et al. ($Nf = 1580$), resulting in a slower predicted bubble velocity (in the form of Fr_θ).

5. Conclusions

In this study, the motion of single Taylor bubbles through stagnant Newtonian fluids in vertical and inclined concentric annuli has been

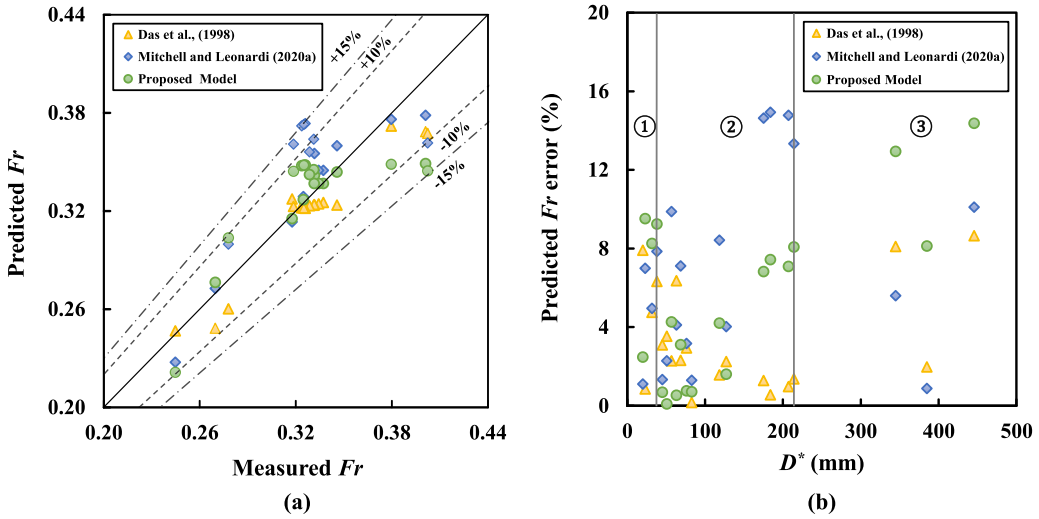


Fig. 12. Comparison between the proposed correlation and existing models with the data in Table 5. (a) cross-plot of measure and predicted Fr; (b) Predicted Fr error against D^* .

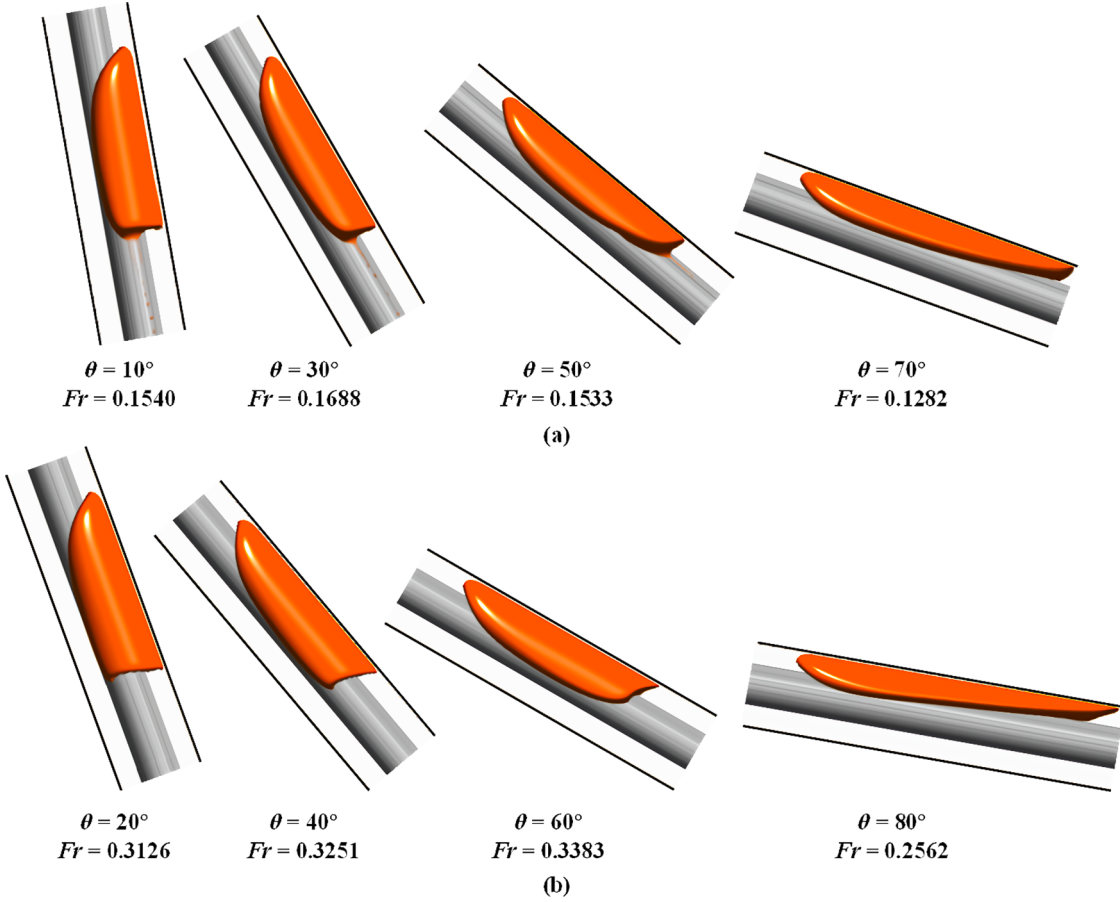


Fig. 13. Fully-developed bubble shape (side view) and Fr in inclined annulus. (a) $Eo = 20$, $Nf = 40$; (b) $Eo = 60$, $Nf = 80$.

numerically studied using three-dimensional CFD simulations with Volume-of-Fluid (VOF) method. A wide range of fluid properties characterized by the dimensionless Eötvös number $Eo = [10, 300]$, inverse viscosity number $Nf = [40, 320]$ and various inclination angles $\theta = \{10^\circ, 20^\circ, 30^\circ, \dots, 80^\circ\}$ are considered. The effects of those parameters on the main hydrodynamic features including the fully-developed bubble shape and drift velocity are discussed. The following conclusions can be drawn:

- 1 For a constant Eo , when the viscous force on the Taylor bubble diminishes due to the increase of the Nf , the Fr increases. For a fixed Nf , surface tension strongly impacts Fr for $Eo = [10, 20]$. Fr eventually reaches a plateau as Eo approaches 100, and this critical value of Eo increases with decreasing Nf .
- 2 The bubble tail adjacent to the liquid bridge stretched with the increase of Nf , eventually breaking off and entraining small bubbles at $Nf = 320$ due to turbulent motion of the low viscosity fluid in the

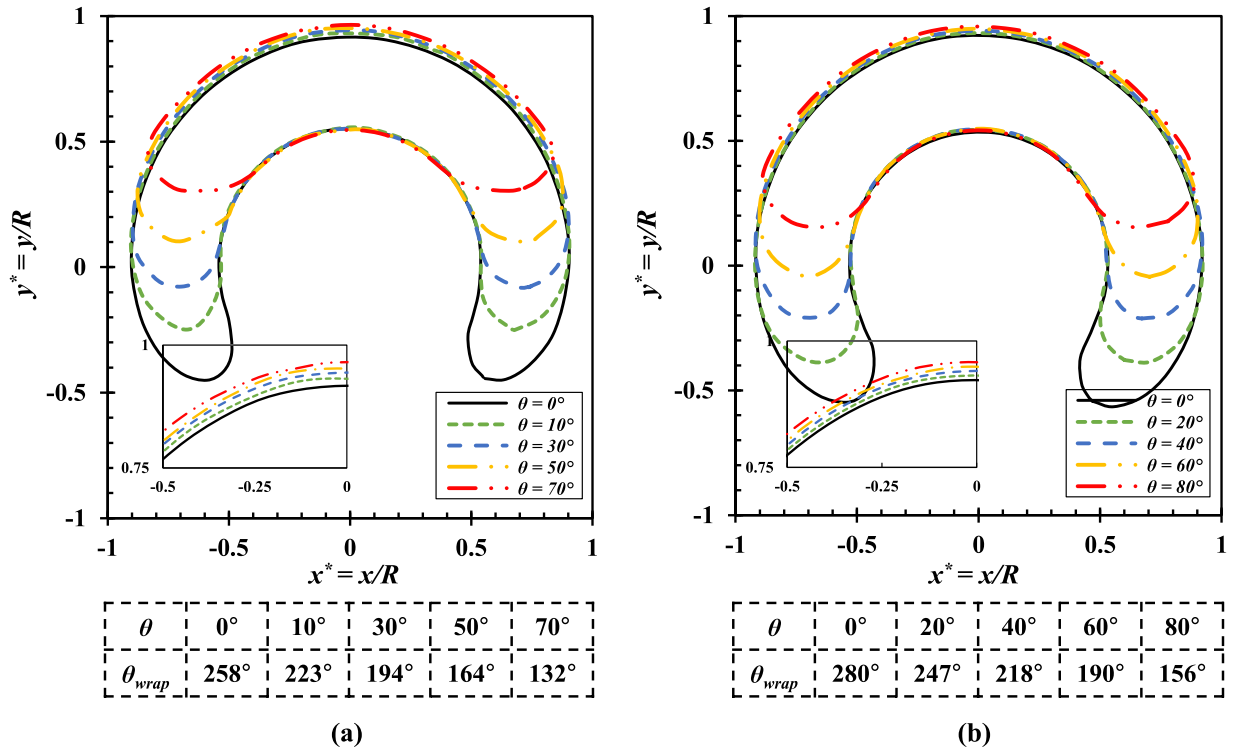


Fig. 14. Cross-sectional Taylor bubble profile dependence on inclination angle. (a) $Eo = 20$, $Nf = 40$; (b) $Eo = 60$, $Nf = 80$.

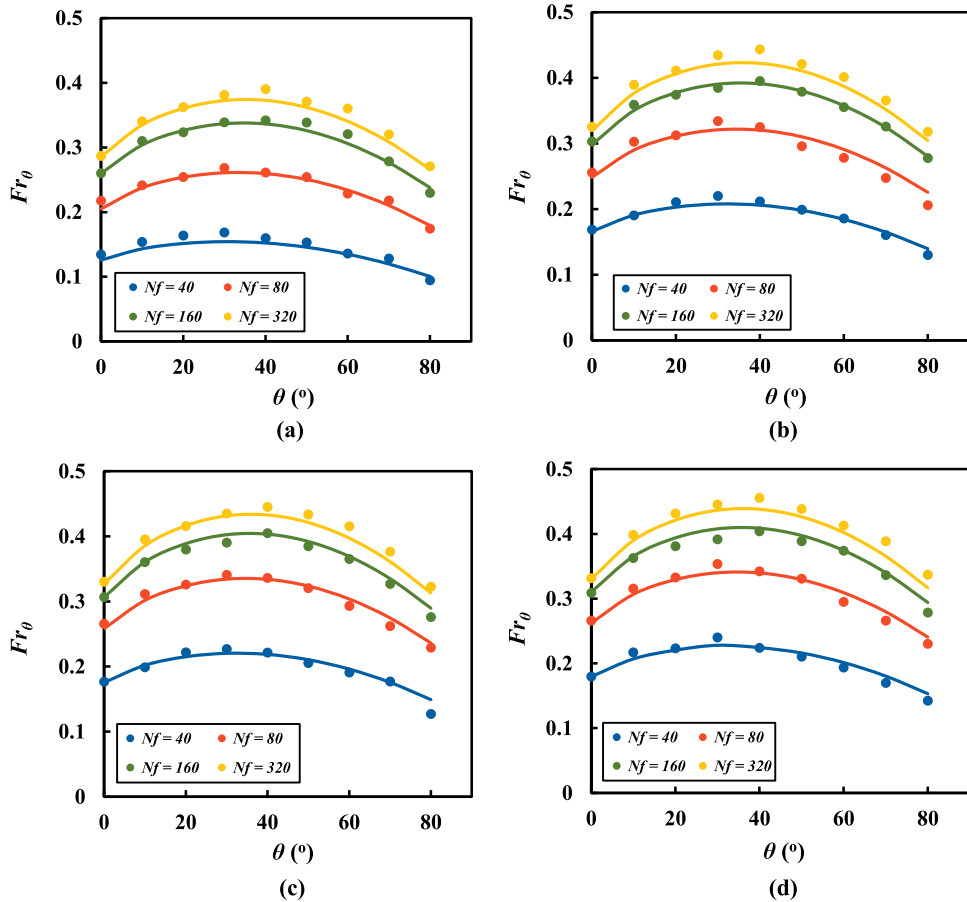


Fig. 15. Fr_0 predictions – numerical simulation (●) versus proposed correlation [Eq. (26)] (—). (a) $Eo = 20$; (b) $Eo = 60$; (c) $Eo = 100$; (d) $Eo = 140$.

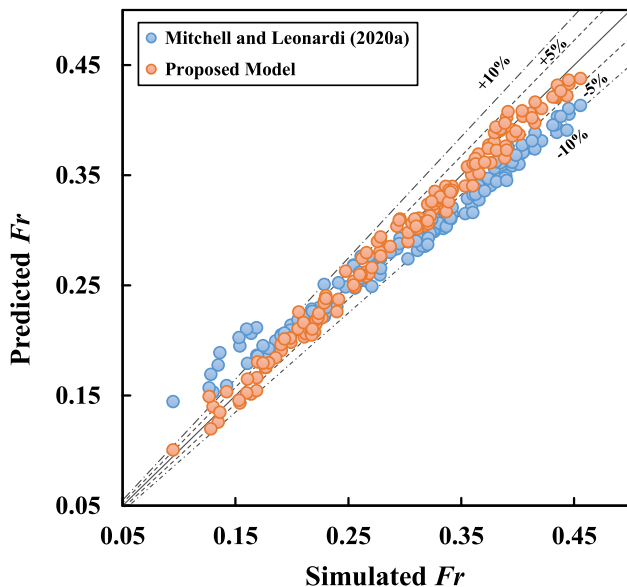


Fig. 16. Comparison of the proposed model [Eq. (26)] with Mitchell and Leonardi's model [Eq. (25)].

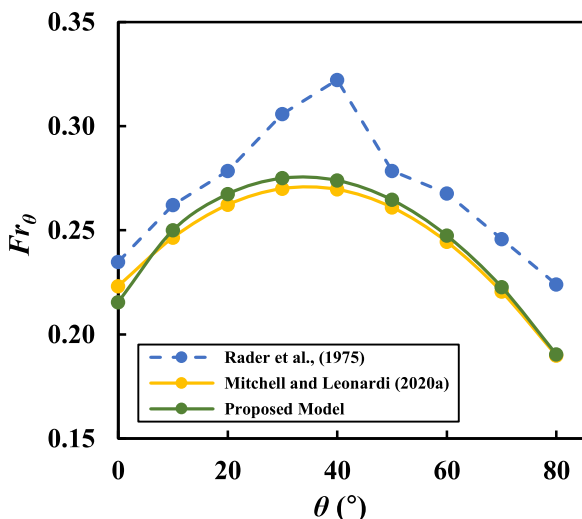


Fig. 17. The experimental Fr_θ from Rader et al., (1975) and calculated values from Eq. (25) and Eq. (26) as a function of θ .

Taylor bubble's wake. Increasing Eo makes the bubble more deformable due to the decrease in surface tension. This results in a longer bubble and a transition of the Taylor bubble's trailing edge from a convex ($Eo = 10$) to a concave shape.

3 A correlation [Eq. (24)] for vertical Fr as a function of Eo and Nf is proposed and compared against 66 numerical simulations, resulting in an average error of 2.13%. The same correlation yields a 5.52% average error for 20 air-water experimental results available in the literature. Relative to the experimental literature data, larger average errors are observed for $D^* \leq 45$ mm (7.38%) and for $D^* \geq 344.9$ mm (11.82%). Whereas for $45 \text{ mm} \leq D^* \leq 214$ mm, the correlation exhibits better performance with an average error of 3.5%. In this last range of D^* , our correlation shows improved performance relative to Mitchell and Leonardi's [Eq. (10)], whose average error is 7.64%.

4 Inclination angle θ has a significant influence on the bubble shape. Increasing θ results in the bubble nose becoming more streamlined and the tail getting elongated due to a shifting of buoyancy forces

from longitudinal to transverse. This forces a reduction in the cross-sectional area of the bubble, which results in bubble elongation and a linear decrease in the wrap angle.

- 5 The cross-sectional area occupied by the bubble is substantially reduced in an inclined annulus, thus reducing drag as inclination increases. This results in an initial increase in Fr , followed by its reduction as longitudinal buoyancy forces decline with increasing inclination. Depending on rheology, Fr is usually maximized at $\theta = 30^\circ - 60^\circ$.
- 6 A correlation [Eq. (26)] for Fr in an inclined orientation is proposed and successfully evaluated by numerical observations. Due to the significantly higher viscosity of the fitted data set ($Nf = 40-320$), the model tends to under-predict the lower viscosity experimental data of Rader et al., (1975) by 8.75%.

CRediT authorship contribution statement

Yixin Liu: Conceptualization, Methodology, Software, Validation, Formal analysis, Writing – original draft. **Even M. Ozbayoglu:** Writing – review & editing, Supervision. **Eric R. Upchurch:** Formal analysis, Writing – review & editing. **Silvio Baldino:** Writing – review & editing.

Declaration of Competing Interest

The authors declared that they have no conflicts of interest to this work. We declare that we do not have any commercial or associative interest that represents a conflict of interest in connection with the work submitted.

Data Availability

Data will be made available on request.

Acknowledgments

The authors would like to thank Dr. Enass Massoud from Arab Academy for Science, Technology and Maritime Transport and Dr. Chuan Xie from Southwest Petroleum University for their technical support with the CFD model development.

References

- Abubakar, H. and Matar, O., 2021. Taylor bubble motion in stagnant and flowing liquids in vertical pipes. Part I: steady-states. arXiv preprint arXiv:2109.09091.
- Agarwal, V., Jana, A.K., Das, G., Das, P.K., 2007. Taylor bubbles in liquid filled annuli: some new observations. Phys. Fluids 19 (10), 108105.
- Alves, I.N., Shoham, O., Taitel, Y., 1993. Drift velocity of elongated bubbles in inclined pipes. Chem. Eng. Sci. 48 (17), 3063–3070.
- Araujo, J.D.P., Miranda, J.M., Pinto, A.M.F.R., Campos, J.B.L.M., 2012. Wide-ranging survey on the laminar flow of individual Taylor bubbles rising through stagnant Newtonian liquids. Int. J. Multiphase Flow 43, 131–148.
- Barnea, D., Shemer, L., 1986. Rise velocity of large bubbles in stagnant liquid in non-circular ducts. Int. J. Multiphase Flow 12 (6), 1025–1027.
- Bendiksen, K.H., 1984. An experimental investigation of the motion of long bubbles in inclined tubes. Int. J. Multiphase Flow 10 (4), 467–483.
- Benjamin, T.B., 1968. Gravity currents and related phenomena. J. Fluid Mech. 31 (2), 209–248.
- Brackbill, J.U., Kothe, D.B., Zemach, C., 1992. A continuum method for modeling surface tension. J. Comput. Phys. 100 (2), 335–354.
- Brown, R.A.S., 1965. The mechanics of large gas bubbles in tubes: I. Bubble velocities in stagnant liquids. Can. J. Chem. Eng. 43 (5), 217–223.
- Bugg, J.D., Saad, G.A., 2002. The velocity field around a Taylor bubble rising in a stagnant viscous fluid: numerical and experimental results. Int. J. Multiphase Flow 28 (5), 791–803.
- Caetano, E.F., Shoham, O., Brill, J.P., 1992a. Upward vertical two-phase flow through an annulus—part I: single-phase friction factor, Taylor bubble rise velocity, and flow pattern prediction. J. Energy Resour. Technol. 114.
- Caetano, E.F., Shoham, O., Brill, J.P., 1992b. Upward vertical two-phase flow through an annulus—part II: modeling bubble, slug, and annular flow. J. Energy Resour. Technol. 114.

- Carew, P.S., Thomas, N.H., Johnson, A.B., 1995. A physically based correlation for the effects of power law rheology and inclination on slug bubble rise velocity. *Int. J. Multiphase Flow* 21 (6), 1091–1106.
- Cook, M., Behnia, M., 2001. Bubble motion during inclined intermittent flow. *Int. J. Heat Fluid Flow* 22 (5), 543–551.
- Das, G., Das, P.K., Purohit, N.K., Mitra, A.K., 1998. Rise velocity of a Taylor bubble through concentric annulus. *Chem. Eng. Sci.* 53 (5), 977–993.
- Davies, R.M., Taylor, G.I., 1950. The mechanics of large bubbles rising through extended liquids and through liquids in tubes. In: Proceedings of the Royal Society of London. Series A. Mathematical and Physical Sciences, 200, pp. 375–390.
- Dumitrescu, D.T., 1943. Strömung an einer luftblase im senkrechten rohr. *ZAMM-J. Appl. Math. Mech./Z. Angew. Math. Mech.* 23 (3), 139–149.
- Fabre, J., 2016. A long bubble rising in still liquid in a vertical channel: a plane inviscid solution. *J. Fluid Mech.* 797.
- Firouzi, M., Towler, B., Rufford, T.E., 2016. Developing new mechanistic models for predicting pressure gradient in coal bed methane wells. *J. Nat. Gas Sci. Eng.* 33, 961–972.
- Friedemann, C., Mortensen, M., Nossen, J., 2019. Gas-liquid slug flow in a horizontal concentric annulus, a comparison of numerical simulations and experimental data. *Int. J. Heat Fluid Flow* 78, 108437.
- Friedemann, C., Mortensen, M., Nossen, J., 2020. Two-phase flow simulations at 0–40° inclination in an eccentric annulus. *Int. J. Heat Fluid Flow* 83, 108586.
- Funada, T., Joseph, D.D., Maehara, T., Yamashita, S., 2005. Ellipsoidal model of the rise of a Taylor bubble in a round tube. *Int. J. Multiphase Flow* 31 (4), 473–491.
- Gokcal, B., Al-Sarkhi, A.S., Sarica, C., 2009. Effects of high oil viscosity on drift velocity for horizontal and upward inclined pipes. SPE Projects, Facil. Constr. 4 (02), 32–40.
- Grace, J.R., Harrison, D., 1967. The influence of bubble shape on the rising velocities of large bubbles. *Chem. Eng. Sci.* 22 (10), 1337–1347.
- Griffith, P., 1964. The prediction of low-quality boiling voids. *J. Heat Transfer* 86 (3), 327–333.
- Gutiérrez, E., Balcázar, N., Bartrons, E., Rigola, J., 2017. Numerical study of Taylor bubbles rising in a stagnant liquid using a level-set/moving-mesh method. *Chem. Eng. Sci.* 164, 158–177.
- Hasan, A.R., Kabir, C.S., 1988. Predicting multiphase flow behavior in a deviated well. *SPE Prod. Eng.* 3 (04), 474–482.
- Hasan, A.R., Kabir, C.S., 1992. Two-phase flow in vertical and inclined annuli. *Int. J. Multiphase Flow* 18 (2), 279–293.
- Hirt, C.W., Nichols, B.D., 1981. Volume of fluid (VOF) method for the dynamics of free boundaries. *J. Comput. Phys.* 39 (1), 201–225.
- Hua, J., Lou, J., 2007. Numerical simulation of bubble rising in viscous liquid. *J. Comput. Phys.* 222 (2), 769–795.
- Jeyachandran, B.C., Gokcal, B., Al-Sarkhi, A., Sarica, C., Sharma, A.K., 2012. Drift-velocity closure relationships for slug two-phase high-viscosity oil flow in pipes. *SPE J.* 17 (02), 593–601.
- Joseph, D.D., 2003. Rise velocity of a spherical cap bubble. *J. Fluid Mech.* 488, 213.
- Kang, C.W., Quan, S., Lou, J., 2010. Numerical study of a Taylor bubble rising in stagnant liquids. *Phys. Rev. E* 81 (6), 066308.
- Kawaiji, M., DeJesus, J.M., Tudose, G., 1997. Investigation of flow structures in vertical slug flow. *Nucl. Eng. Des.* 175 (1-2), 37–48.
- Kelessidis, V.C., Dukler, A.E., 1990. Motion of large gas bubbles through liquids in vertical concentric and eccentric annuli. *Int. J. Multiphase Flow* 16 (3), 375–390.
- Keshavarzi, G., Pawell, R.S., Barber, T.J., Yeoh, G.H., 2014. Transient analysis of a single rising bubble used for numerical validation for multiphase flow. *Chem. Eng. Sci.* 112, 25–34.
- Liné, A., Belt, R., Munoz, J.M., Allain, O., Guegan, D., 2013. Data processing of full 3D numerical simulation of slug flow to improve unit cell model. In: 16th International Conference on Multiphase Production Technology. OnePetro.
- Liu, Y., Tong, T.A., Ozbayoglu, E., Yu, M., Upchurch, E., 2020. An improved drift-flux correlation for gas-liquid two-phase flow in horizontal and vertical upward inclined wells. *J. Pet. Sci. Eng.* 195, 107881.
- Liu, Y., Upchurch, E.R., Ozbayoglu, E.M., 2021. Experimental study of single Taylor bubble rising in stagnant and downward flowing non-Newtonian fluids in inclined pipes. *Energies* 14 (3), 578.
- Liu, Y., Upchurch, E.R., Ozbayoglu, E.M., 2022. Experimental and theoretical studies on Taylor bubbles rising in stagnant Non-Newtonian fluids in inclined non-concentric annuli. *Int. J. Multiphase Flow* 147, 103912.
- Lizarraga-Garcia, E., Buongiorno, J., Al-Safran, E., 2021. Computational fluid dynamics (CFD) simulations of Taylor bubbles in vertical and inclined pipes with upward and downward liquid flow. *SPE J.* 26 (06), 3832–3847.
- Lizarraga-Garcia, E., Buongiorno, J., Al-Safran, E., Lakehal, D., 2017. A broadly-applicable unified closure relation for Taylor bubble rise velocity in pipes with stagnant liquid. *Int. J. Multiphase Flow* 89, 345–358.
- Llewellyn, E.W., Del Bello, E., Taddeucci, J., Scarlato, P., Lane, S.J., 2012. The thickness of the falling film of liquid around a Taylor bubble. In: Proceedings of the Royal Society A: Mathematical, Physical and Engineering Sciences, 468, pp. 1041–1064.
- Lou, W., Wang, Z., Guo, B., Pan, S., Liu, Y., Sun, B., 2022a. Numerical analysis of velocity field and energy transformation, and prediction model for Taylor bubbles in annular slug flow of static power law fluid. *Chem. Eng. Sci.*, 117396
- Lou, Wenqiang, Zhiyuan, W.A.N.G., Pengfei, L.I., Xiaohui, S.U.N., Baojiang, S.U.N., Yaxin, L.I.U., Dalin, S.U.N., 2022. Wellbore drift flow relation suitable for full flow pattern domain and full dip range. *Pet. Expl. Dev.* 49 (3), 694–706.
- Lou, W., Wang, Z., Pan, S., Sun, B., Zhang, J., Chen, W., 2020. Prediction model and energy dissipation analysis of Taylor bubble rise velocity in yield stress fluid. *Chem. Eng. J.* 396, 125261.
- Lu, X., Prosperetti, A., 2009. A numerical study of Taylor bubbles. *Ind. Eng. Chem. Res.* 48 (1), 242–252.
- Luo, C., Cao, Y., Liu, Y., Zhong, S., Zhao, S., Liu, Z., Liu, Y., Zheng, D., 2022. Experimental and modeling investigation on gas-liquid two-phase flow in horizontal gas wells. *J. Energy Resour. Technol.* 1–13.
- Majumdar, A., Das, P.K., 2019. Rise of Taylor bubbles through power law fluids-analytical modelling and numerical simulation. *Chem. Eng. Sci.* 205, 83–93.
- Mao, Z.S., Dukler, A.E., 1990. The motion of Taylor bubbles in vertical tubes. I. A numerical simulation for the shape and rise velocity of Taylor bubbles in stagnant and flowing liquid. *J. Comput. Phys.* 91 (1), 132–160.
- Massoud, E.Z., Xiao, Q., El-Gamal, H.A., 2020. Numerical study of an individual Taylor bubble drifting through stagnant liquid in an inclined pipe. *Ocean Eng.* 195, 106648.
- Massoud, E.Z., Xiao, Q., El-Gamal, H.A., Teamah, M.A., 2018. Numerical study of an individual Taylor bubble rising through stagnant liquids under laminar flow regime. *Ocean Eng.* 162, 117–137.
- Mitchell, T., Holzer, M., Schwarzmeier, C., Bauer, M., Rüde, U., Leonardi, C., 2021. Stability assessment of the phase-field lattice Boltzmann model and its application to Taylor bubbles in annular piping geometries. *Phys. Fluids* 33 (8), 083325.
- Mitchell, T., Leonardi, C., 2020a. Development of closure relations for the motion of Taylor bubbles in vertical and inclined annular pipes using high-fidelity numerical modeling. *Phys. Fluids* 32 (6), 063306.
- Mitchell, T., Leonardi, C., 2020b. On the rise characteristics of Taylor bubbles in annular piping. *Int. J. Multiphase Flow* 130, 103376.
- Moreiras, J., Pereyra, E., Sarica, C., Torres, C.F., 2014. Unified drift velocity closure relationship for large bubbles rising in stagnant viscous fluids in pipes. *J. Pet. Sci. Eng.* 124, 359–366.
- Nogueira, S., Riethmuler, M.L., Campos, J.B.L.M., Pinto, A.M.F.R., 2006. Flow in the nose region and annular film around a Taylor bubble rising through vertical columns of stagnant and flowing Newtonian liquids. *Chem. Eng. Sci.* 61 (2), 845–857.
- Ohta, M., Tsuji, M., Yoshida, Y., Sussman, M., 2008. The transient dynamics of a small bubble rising in a low Morton number regime. *Chem. Eng. Technol.* 31 (9), 1350–1357.
- Petalas, N., Aziz, K., 2000. A mechanistic model for multiphase flow in pipes. *J. Can. Pet. Technol.* (06), 39.
- Polonsky, S., Shemer, L., Barnea, D., 1999. The relation between the Taylor bubble motion and the velocity field ahead of it. *Int. J. Multiphase Flow* 25 (6-7), 957–975.
- Quan, S., 2011. Co-current flow effects on a rising Taylor bubble. *Int. J. Multiphase Flow* 37 (8), 888–897.
- Rader, D.W., Bourgoyne Jr, A., Ward, R.H., 1975. Factors affecting bubble-rise velocity of gas kicks. *J. Pet. Technol.* 27 (05), 571–584.
- Rohilla, L., Das, A.K., 2017. On transformation of a Taylor bubble to an asymmetric sectorial wrap in an annuli. *Ind. Eng. Chem. Res.* 56 (48), 14384–14395.
- Rohilla, L., Das, A.K., 2019. Experimental study on the interfacial evolution of Taylor bubble at inception of an annulus. *Ind. Eng. Chem. Res.* 58 (6), 2356–2369.
- Sadatomi, M., Sato, Y., Saruwatari, S., 1982. Two-phase flow in vertical noncircular channels. *Int. J. Multiphase Flow* 8 (6), 641–655.
- Shosho, C.E., Ryan, M.E., 2001. An experimental study of the motion of long bubbles in inclined tubes. *Chem. Eng. Sci.* 56 (6), 2191–2204.
- Sousa, R.G., Pinto, A.M.F.R., Campos, J.B.L.M., 2006. Effect of gas expansion on the velocity of a Taylor bubble: PIV measurements. *Int. J. Multiphase Flow* 32 (10-11), 1182–1190.
- Taha, T., Cui, Z.F., 2006. CFD modelling of slug flow in vertical tubes. *Chem. Eng. Sci.* 61 (2), 676–687.
- Viana, F., Pardo, R., Yáñez, R., Trallero, J.L., Joseph, D.D., 2003. Universal correlation for the rise velocity of long gas bubbles in round pipes. *J. Fluid Mech.* 494 (379-398).
- Weber, M.E., Alarie, A., Ryan, M.E., 1986. Velocities of extended bubbles in inclined tubes. *Chem. Eng. Sci.* 41 (9), 2235–2240.
- White, E.T., Beardmore, R.H., 1962. The velocity of rise of single cylindrical air bubbles through liquids contained in vertical tubes. *Chem. Eng. Sci.* 17 (5), 351–361.
- Xie, C., Liu, Y., Li, X., Wang, G., Wang, Q., Zeng, F., 2022a. Numerical and orthogonal study on optimization analysis of structure parameters of bubble breaker for electrical submersible pump system. *J. Energy Resour. Technol.* 144 (1).
- Xie, C., Liu, Y., Li, X., Wu, N., Luo, C., Zeng, F.B., 2022b. A novel comprehensive model for predicting production of downhole choke wells. *Fuel* 313, 122944.
- Zhu, H., Zhu, J., Rutter, R., Zhang, H.Q., 2019. A numerical study on erosion model selection and effect of pump type and sand characters in electrical submersible pumps by sandy flow. *J. Energy Resour. Technol.* 141 (12).
- Zukoski, E.E., 1966. Influence of viscosity, surface tension, and inclination angle on motion of long bubbles in closed tubes. *J. Fluid Mech.* 25 (4), 821–837.